Hindawi
Modelling and Simulation in Engineering
Volume 2023, Article ID 9655548, 13 pages
https://doi.org/10.1155/2023/9655548

Research Article

Mechanical Behavior of Chain-Link Wire Nets under Pressure from a Warhead: Quasistatic Experiments and Simulations

Min Wang,[1,2] **Shuai Zhou**,[1] **and Qilin Huang**[1]

[1]*Department of Military Facilities, Army Logistics Academy, Chongqing 401311, China*
[2]*Key laboratory of Military Underground Architectural Engineering, Army Logistics Academy, Chongqing 401311, China*

Correspondence should be addressed to Min Wang; wangmin198217@163.com

Received 29 March 2023; Revised 26 May 2023; Accepted 5 June 2023; Published 21 June 2023

Academic Editor: Chao Bao

Wire nets woven from high-strength steel wires have been used as applique armor against attack by short-range weapons. In this study, the mechanical behavior of chain-link wire nets under pressure from a warhead was investigated by quasistatic experiments and simulations. First, the new rig, the warhead device, and the wire nets were designed; pressure tests were conducted; and the deformation, fracture of the wire nets, and pressure force vs. displacement curves were obtained and analyzed. Then, the numerical approach and Finite element (FE) model were developed, considering the contacts between the steel wires in the inner connections, the contacts between the warhead and the mesh of the wire nets, and the fracture of the steel wire material. By comparison with the experimental data, the numerical approach and FE model are shown to be reliable in predicting the behavior of the wire nets under pressure from a warhead. Finally, the parameters of the wire net size and the mesh angles were further investigated by using the validated numerical approach and FE model, and suggestions for the initial design of the wire nets are discussed.

1. Introduction

Wire nets woven by steel wire are three-dimensional metallic fabric structures, and various wire nets with different fabric techniques and geometry features have been developed (Figure 1), such as chain-link wire nets with diamond-shaped or ring features, double-twisted wire nets with hexagonal features, and welded wire nets with rectangle features. Because of their lightness and unique mechanical properties compared to steel sheets or other protective devices [1, 2], wire nets have been used in many engineering applications. In natural hazard protection systems, wire nets are used as key components for rockfall protection barriers [3, 4], slope reinforcement [5], and ground surface support systems [6]. In thin-walled security screens, wire nets are used as security screen doors and window grills against unauthorized intrusions and windborne debris impacts [7, 8]. In protective engineering applications, wire nets are employed to reinforce the concrete slab to protect it against explosion and projectile impacts [9, 10]. With the increase in the strength and ductility of steel wires, wire nets woven from high-strength steel wires have been used as applique armor (Figure 2) against attacks by short-range weapons such as rifle propelled grenades (RPGs), mortar shells, or heavy machine guns [11, 12].

Many previous studies on the static mechanical properties of wire nets woven by high-strength steel wire were conducted, and these studies mainly focused on the natural hazard protection field and simulated the load deduced by shallow landslides and rock block impact conditions, including quasistatic in-plane tensile experiments [13, 14], quasistatic out-of-plane pressure experiments [15, 16], and supplementary numerical simulation [17–19]. Figure 3 shows the fracture of the wire nets under short-range weapon attacks and rigid warhead impacts with low velocity [12, 20]. The contact area of the wire nets impacted by the short-range weapons or rigid warheads is limited to a single mesh, and

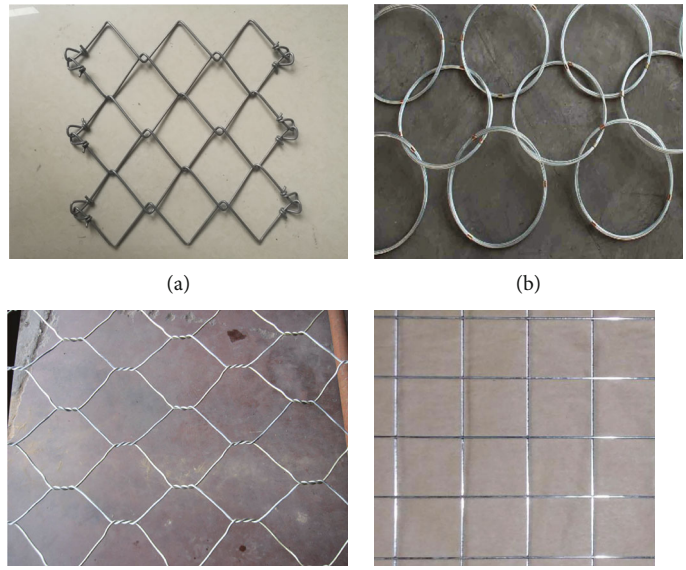

(a) (b) (c) (d)

Figure 1: Wire nets woven by the steel wires: (a) chink-link wire nets; (b) ring nets; (c) double-twisted wire nets; (d) welded-wire nets.

(a) (b)

Figure 2: The applique armor composed of wire nets woven from high-strength steel wires: (a) chink-link wire nets; (b) parallel wire fences.

this phenomenon is much different from those presented in studies simulating shallow landslides and rockfalls. To improve the efficiency of wire nets in intercepting short-range weapons, the static mechanical behavior of wire nets under quasistatic pressure from a warhead is a basic research work, which is important for the initial design of wire nets to resist attack by short-range weapons. To date, little attention has been given to the mechanical behavior of chain-link wire nets under quasistatic pressure from a warhead. Due to the abovementioned research gaps, the aims of this paper are threefold, as follows:

(i) To design and conduct quasistatic experiments of wire nets pressurized by warheads based on the results from short-weapon attack tests and rigid warhead impact tests and then investigate the mechanical behavior of the wire nets.

(ii) To develop the numerical approach and finite element (FE) model to simulate the wire nets pressurized by a warhead and validate the numerical simulation results by comparison with the experimental data.

(iii) To discuss the wire nets sizes and mesh angles by using FE simulation and then to discuss suggestions of an initial design for the wire nets.

2. Experimental Methodology

Several testing rigs for wire nets under out-of-plane pressure were developed [6, 15, 16]. Different from previous rigs used in out-of-plane pressure tests for wire nets, a new testing rig (Figure 4(a)) has been developed. The new rig can apply pretension on the wire nets to avoid any possible sag in the initial testing stage. The height of the rig is 1.5 m, and the length and width of the rig are 2×2 m. The low parts of the rig are composed of 4 plane sheets and 4 I-beams, which are connected to the counterforce grooves, the middle parts of the rig are composed of 12 I-beams, and the upper parts (Figure 4(b)) of the rig are composed of sliding connections and U-type connectors. Rectangular wire nets of approximately 1×1 m could be installed on the rig using U-type

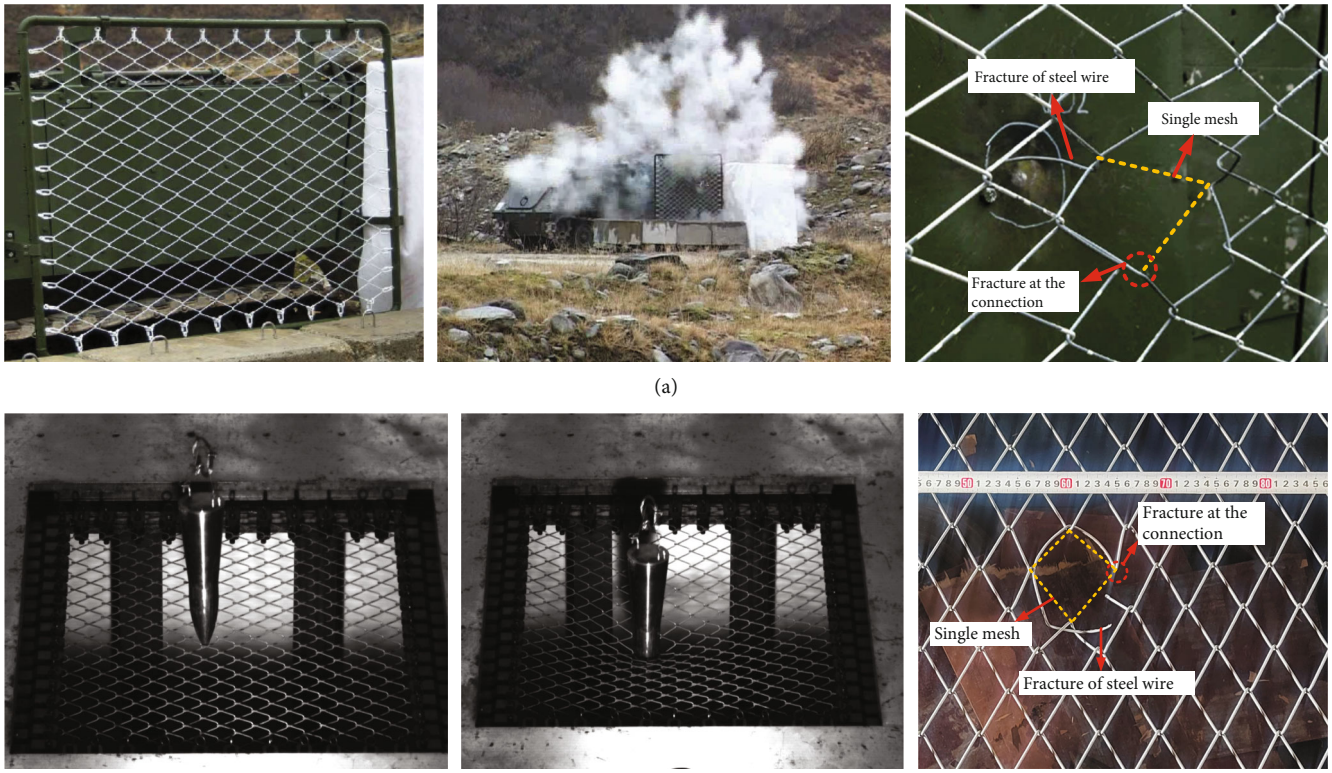

FIGURE 3: The fractures of the wire nets under short-weapon attacks and rigid warhead impacts with low velocity: (a) wire nets attacked by short-weapons; (b) wire nets impacted by rigid warheads.

connectors. The x, y, and z displacements of the wire nets can be constrained by the connectors, and then the sliding connections can apply slight pretension to the wire nets before the tests begin.

According to the shape and dimensions of the short-range weapon (Figure 5), a warhead device of caliber 107 mm is designed and is shown in Figure 6, including warhead, support, and flange plate. The charging and internal structures of the warhead are ignored, and the homogeneous warhead device is manufactured from 304 stainless steel material. The support is designed to lengthen the warhead and apply vertical force, and the flange plate is designed to be connected to the hydraulic presser.

Because the inner cross connections of the wire nets woven by the high-strength steel wire cannot be fixed by electric welding or brazing with a filler metal [21], a fabric technique involving a loose connection type and repeating rhomboidal patterns is used for the chain-link wire nets, and the two wires bent in opposite directions are in loose contact through the inner connections and tied together through knotted connections at the boundaries [14]. The chain-link wire nets are designed, and the drawings of the chain-link wire nets are shown in Figure 7. The detailed dimensions of the chain-link wire nets are shown in Table 1.

To provide the large deformation of the wire nets under pressure from a warhead, a hydraulic presser with a 500 mm large stroke and a measuring range of 20 kN is employed. The warhead was connected to the hydraulic presser through the flange plant by nuts and bolts, and then the warhead needed to be aligned with the center position of the wire net mesh. The longitudinal axis of the warhead and the wire nets needs to be orthogonal during the pressure tests. The setup of the tests is shown in Figure 8. The hydraulic presser pressed the warhead device down at a constant velocity of 10 mm/min, and when the warhead contacted the wire nets, the force and the downing displacement were recorded by the built-in displacement sensor and load sensor of the hydraulic presser. The value of the force and the downing displacement is determined beginning from the warhead contacting the single mesh of the wire nets until the wire nets were fractured. When the wire nets were fractured, the tests were stopped.

3. Experimental Results and Analysis

The pressure testing processes and the deformations of the wire nets are shown in Figure 9. When the warhead device initially penetrated the center mesh, relative displacement occurred between the center mesh and the warhead until the center mesh constrained the warhead, and then the wire nets and the warhead device together moved downward. The deformation of the wire nets included the overall deformation and the local deformation. The overall deformation behavior of the wire nets fits the membrane stretching model, producing a funnel shape, and the local deformation

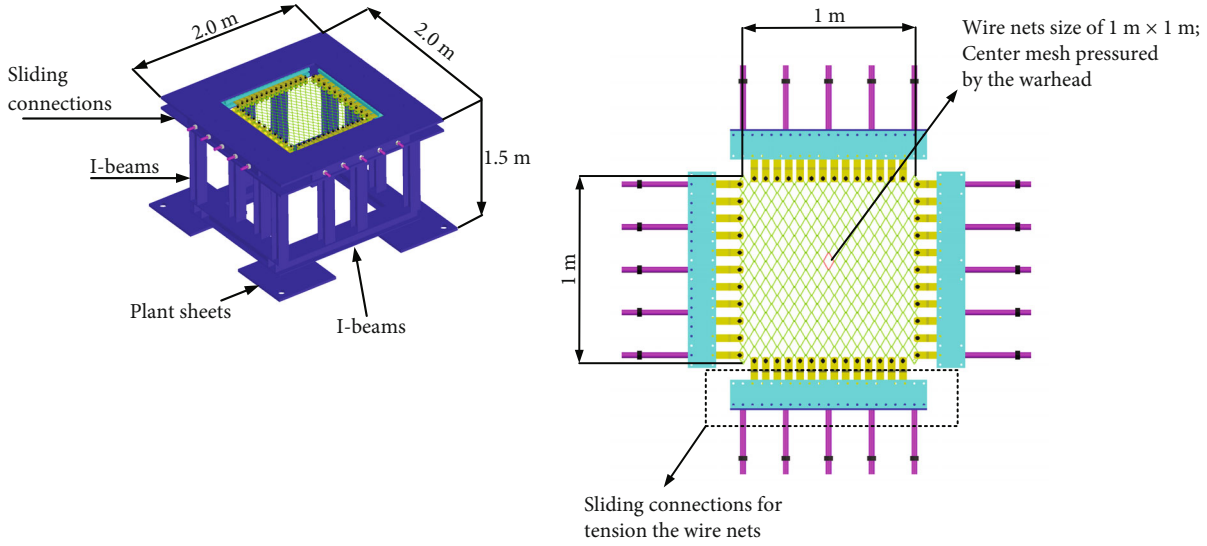

Figure 4: (a) The new testing rig; (b) the details of the upper parts of the rig.

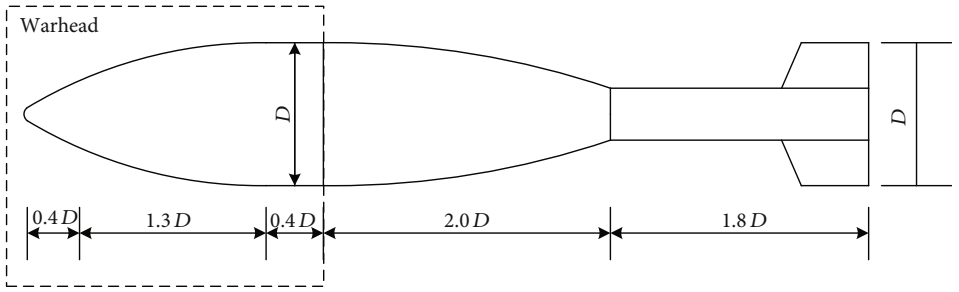

Figure 5: Dimensions of the short-range weapon.

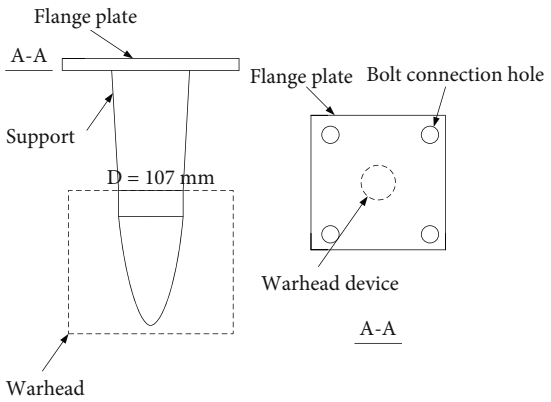

Figure 6: Designed warhead device with a diameter of 107 mm.

referred to the expanded deformation of the center mesh when impacted by the warhead device.

The detailed local deformation and the fracture feature of the wire nets are shown in Figure 10. While the warhead device penetrated the single mesh, circumferential extrusion force was applied to the center mesh by the warhead, and the center mesh gradually deformed in this section in the form of the warhead. The pretensioning of the wire nets before the pressure tests began, together with the pressure on the wire nets applied by the warhead on the center mesh, resulted in symmetrical stress on the wire nets. Therefore, the relative sliding between the steel wires at connections A ~ D was not obvious. There was no significant relative sliding between the two steel wires at inner connections B and D, and only slight sliding at inner connections A and C was observed (Figure 10(a)). For the three-dimensional fabric technology and eccentricity geometry, the strength of the wires in the connections would be slightly decreased for the pre-bending, and the steel wires in the connections resist the bending moment, shear force, and torsional force. The combined stress on the wires at the connections would first exceed the limited stress; therefore, the fracture of the wire nets took place at the connections in the center mesh, and the fracture behavior of the steel wire presented inclined section failure under the combined stress (Figure 10(b)). These phenomena were observed in the two tests. To improve the strength of the wire in the connections, improving the ductility of the wire is an effective solution.

Compared with Figures 3 and 10, whether it was quasi-static pressure tests, low-velocity impact tests, or short-range weapon attack tests, the fractures of the wire nets all

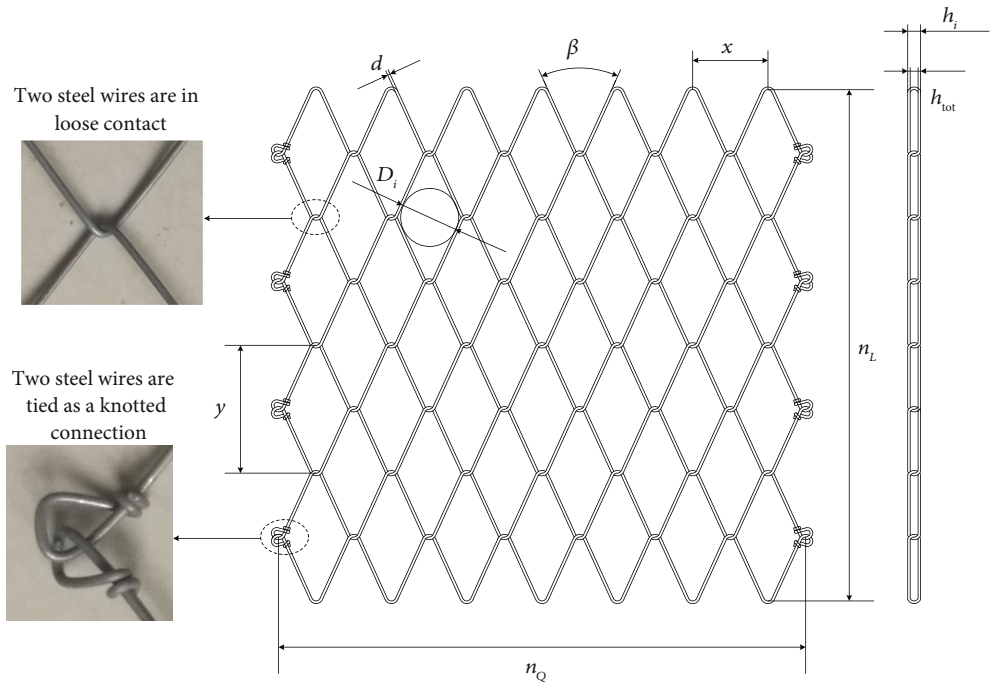

Figure 7: Drawing of the designed chain-link wire net.

Table 1: Detailed dimensions of the designed chain-link wire nets.

Wire net size	$n_Q \cdot n_L = 1000 \cdot 1000$ mm
Wire diameter	$d = 3.0$ mm
Mesh size	$x \cdot y = 59.9 \cdot 93.0$ mm
Incircle diameter of the mesh	$D_i = 45$ mm
Mesh angle	$\alpha = 58.9^\circ$
Total height of the mesh	$h_{tot} = 12.5$ mm
Clearance of the mesh	$h_i = 6.5$ mm
No. of longitudinal meshes	$n_Q = 17$ pcs/m
No. of transversal meshes	$n_L = 11$ pcs/m

occurred at the locations of the connections where the single mesh contacted the warhead. The measured nonlinear pressure force vs. displacement response curves are shown in Figure 11. The tangent of the curves exhibits a progressive increase from 0 to 100 ~ 125 mm, and after the 125 mm displacement, the tangent of the curves remains almost constant until failure.

4. FE Modeling of the Wire Nets under Pressure from the Warhead Device

Although there are several studies on FE modeling of chain-link wire nets for in-plane tensile mechanisms [13, 17, 18], the intricate three-dimensional geometry of the chain-link wire nets and the contacts between the single wires in the inner connections, as well as the contacts between the mesh and the warhead device, makes FE modeling of the wire nets under pressure from a warhead a challenging and distinctive task. Therefore, the chain-link wire nets under pressure from the warhead device were implemented in ANSYS 2022R1 to reproduce the deformation and fracture behavior of the wire nets.

4.1. Numerical Approach and FE Model. There was no fracture or sliding of the knotted connections of the wire nets in the experiments, so the knotted connections in the FE model could be simplified as fixed connections. The warhead device was simplified in the FE model, the flange plant was ignored, and the warhead and support were considered in the FE model. The geometry of the wire nets and the warhead device had much influence on its mechanical behavior, and thus, the imports of the FE model for the chain-link wire nets and the warhead device are in accordance with the measurements used in the experiments.

Because the wires in the inner connections must resist tension, bending, shear, and torsion, beam elements with quadratic order and flexible stiffness behavior were selected for discretizing the wires. Compared to the wires, the stiffness behavior of the warhead devices was rigid, and solid elements with rigid behavior were selected for discretizing the warhead device. The capture curvature method was used, and the curvature normal angle was refined for meshing and capturing the contact behavior of the wires in the connections. A mapped mesh with hard behavior was used for the mesh of the warhead device geometry.

The wires in the inner connections came into contact with each other when the wire nets were pressed by the warhead device. Two main methods have been developed to handle such problems. The multibody coupling algorithm can establish translational constraints and keep free rotation between the contact nodes of the beam elements in the inner connections, but the sliding and contacts between the beam

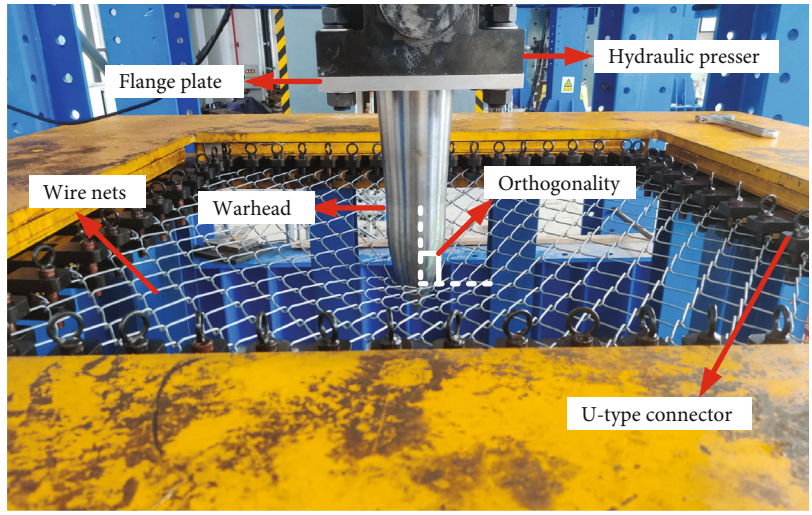

Figure 8: Setup for the pressure tests.

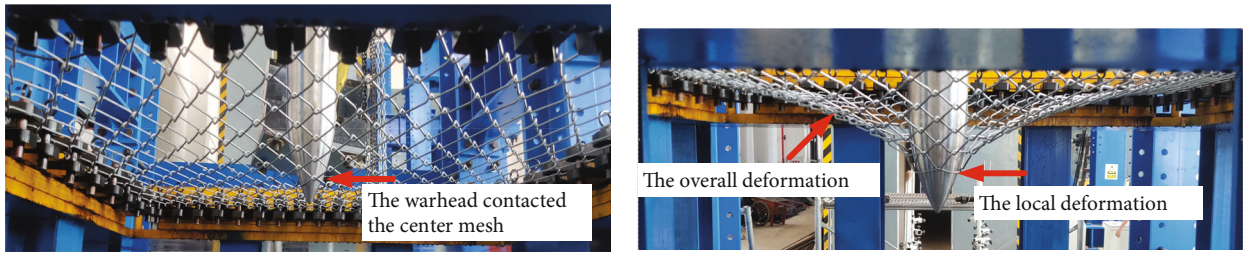

(a) (b)

Figure 9: The testing processes and deformations of the wire nets: (a) the warhead contacting the center mesh; (b) the wire nets and the warhead moving down together.

elements cannot be considered. The implicit beam-to-beam contact algorithm could consider the contacts and sliding of the beam elements in the inner connections, but the normal stiffness in the contacted beam elements would be dramatically changed, which would cause considerable difficulties in convergence or require a more refined mesh in the area of contact and more calculation time. The sliding of the steel wires at the connections was not significant; therefore, to capture the main behavior of the wire nets under pressure by the warhead, a hybrid algorithm was applied to simulate the contact behavior of the wire nets to balance the calculation accuracy, calculation time, and convergence. On the one hand, frictionless beam-to-beam contact was used to simulate the contacts between the beam elements in the inner connections; on the other hand, the multibody coupling algorithm was used to constrain the sliding between the contact nodes of the beam elements. Furthermore, the penetration tolerance factor and normal stiffness factor for the beam-to-beam contact algorithm were refined and optimized.

The multiple to solid contact algorithm was used to simulate contacts and sliding between the warhead device and the wire nets. The frictional coefficient was also considered, and the edgy contact type of line segments was used for the multiple-to-solid contact algorithm. The boundary conditions to simulate the pressure tests were applied in the FE model. The translational freedoms of the simplified knotted connections were constrained, and free rotations were used for modeling the connections between the wire nets and the U-type connectors. Vertical displacement was imposed on the warhead device to perform the quasistatic tests. The FE model of the chain-link wire nets and the warhead device was established and is shown in Figure 12.

4.2. Materials and Fracture. The chain-link wire nets are woven from the high-strength steel wire, and the engineering strain–stress curve of the steel wire under uniaxial tension is shown in Figure 13. As shown in Figure 13, high-strength steel wire is a ductile material with plastic hardening characteristics, the Young's modulus of the steel wire is approximately 1941270 MPa; additionally, the average yield strength (YS, 0.2% offset line) of the wire used is approximately 1550 MPa. The breaking force of the steel wire is approximately 13.58 kN, and the ultimate tensile stress is approximately 1984.66 MPa. The ultimate strain of the steel wire is approximately 0.032. The multilinear isotropic hardening constitutive relationship was employed to describe the steel wire material. For the high nonlinear characteristics of the steel wire material, the plasticity with large strains and large-deflection effects should be considered, and the true

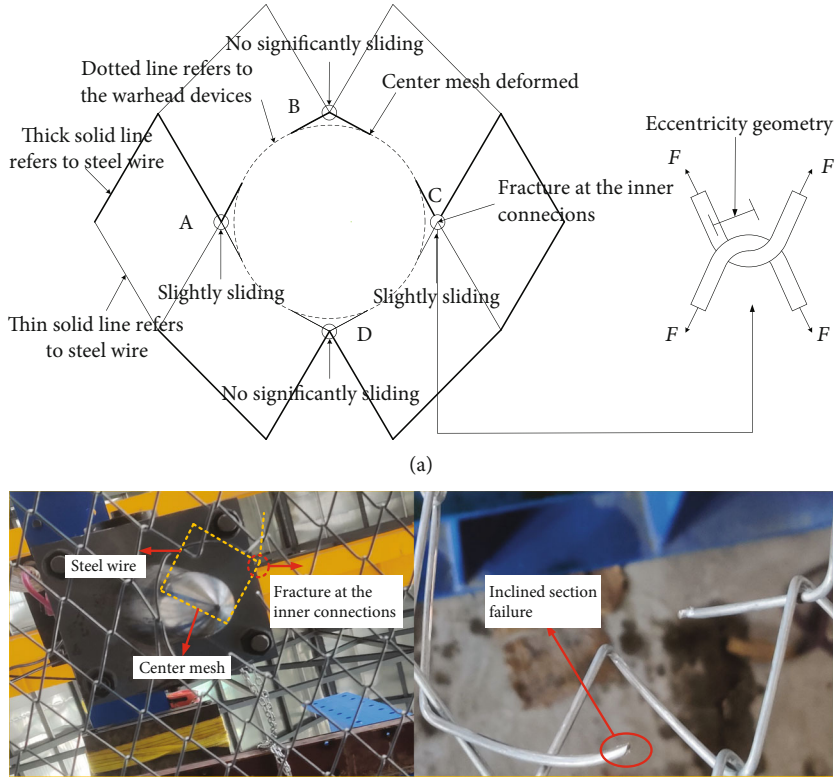

Figure 10: Local deformation of the wire nets: (a) local deformation of the center mesh; (b) fracture feature of the center mesh in the connections.

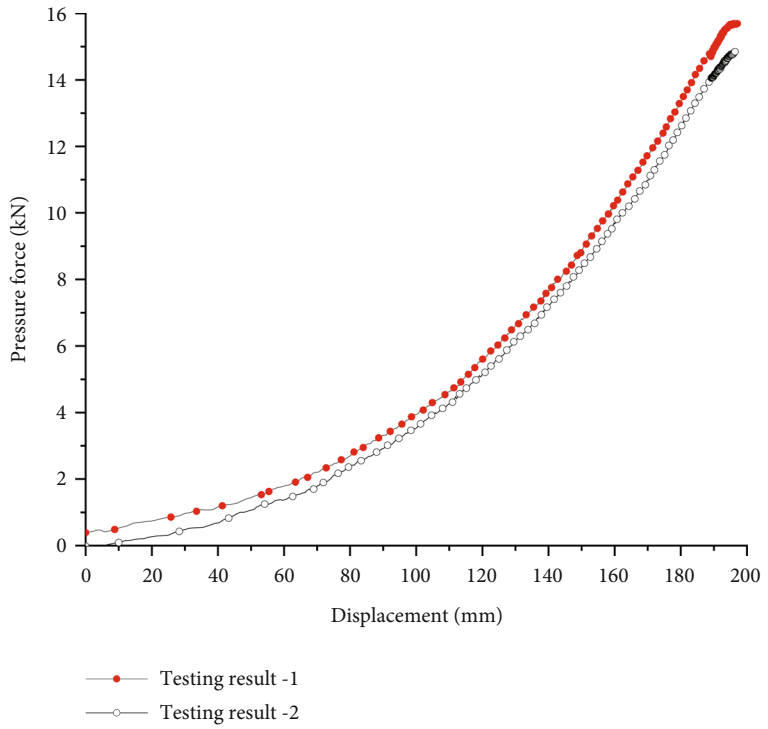

Figure 11: The measured nonlinear pressure force vs. displacement response curves.

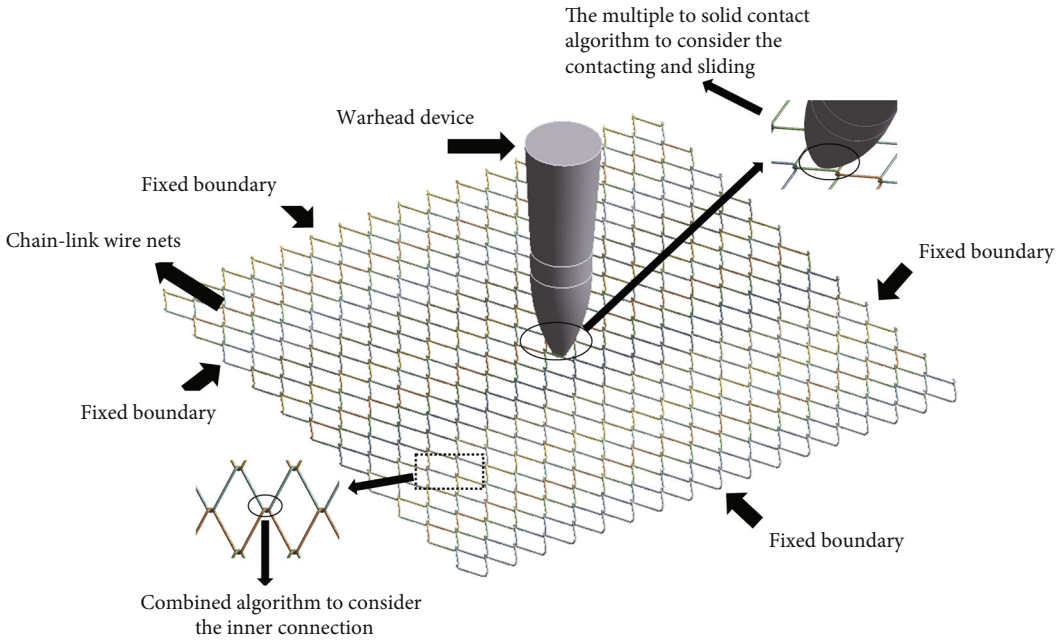

Figure 12: The detailed FE model of a wire net under pressure by a warhead.

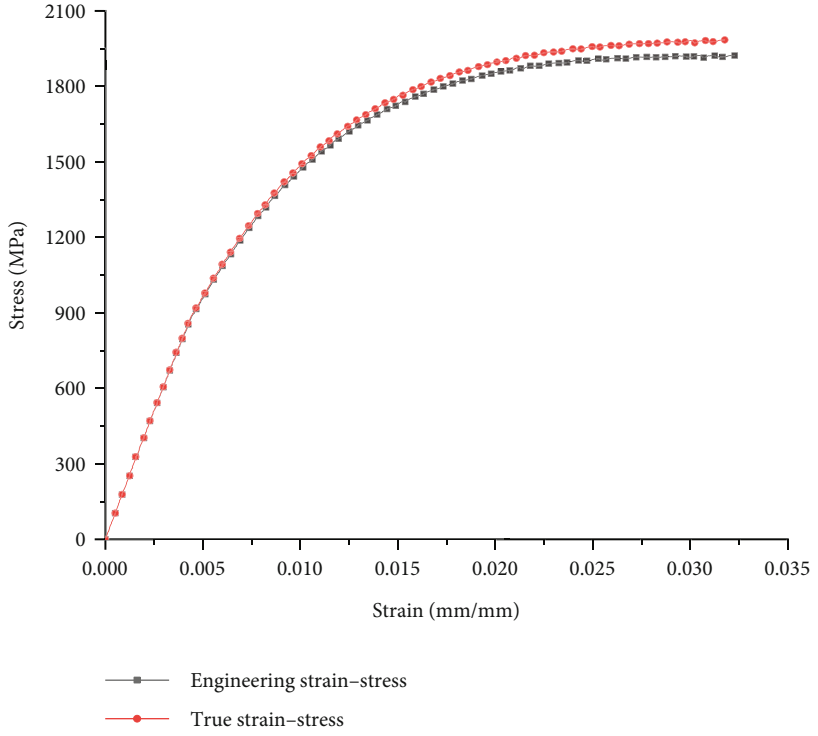

Figure 13: Strain–stress curves of the high-strength steel wire under uniaxial tension.

strain–stress curve of the steel wire material was used in the numerical analysis. The true strain–stress curve of the steel wire material can be obtained by the following formulas [17]:

$$\varepsilon_{\text{true}} = \text{Ln}\left(1 + \varepsilon_{\text{eng}}\right). \quad (1)$$

$$\sigma_{\text{true}} = \sigma_{\text{eng}}\left(1 + \varepsilon_{\text{eng}}\right). \quad (2)$$

where σ_{eng} and ε_{eng} can be derived from the engineering stress–strain curve and are shown in Figure 13.

Although the wires in the connections resisted axial force, bending moments, shear force, and torsional force, the fracturing of the steel wire in the tests was mainly caused

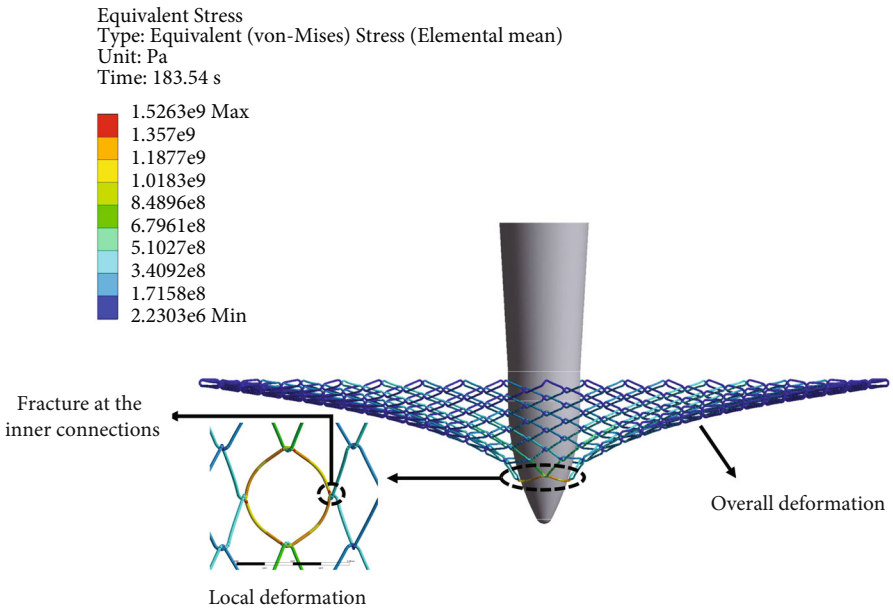

Figure 14: The equivalent stress contour and the deformation of the wire nets.

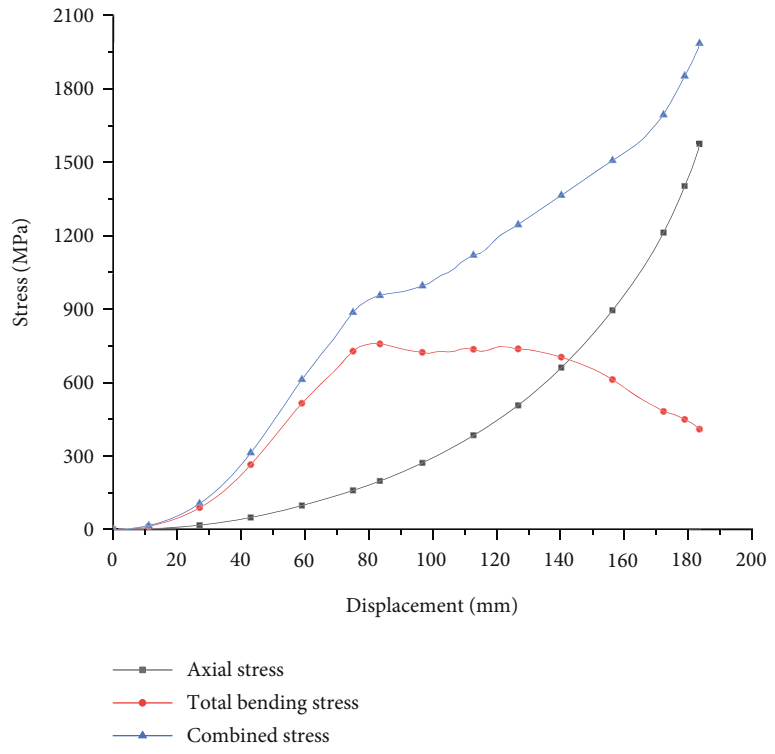

Figure 15: Stress–displacement curves of the failure element.

by the axial force and bending moment. The combined stress law and element birth and death technology were employed to model the fracturing of the steel wires in the tests. The combined stress law includes the axial stress and the bending stress. When the combined stress of the element in the FE model exceeded the limited stress, the element would fail (element death) and the calculation would be stopped. The combined stress law of the steel wire is defined by the following formula:

$$\sigma_1 + \lambda\sigma_2 \leq \sigma_{\text{lim}}. \tag{3}$$

where σ_1 is the axial stress, σ_2 is the total bending stress, σ_1 and σ_2 could be obtained by the numerical simulation; σ_{lim}

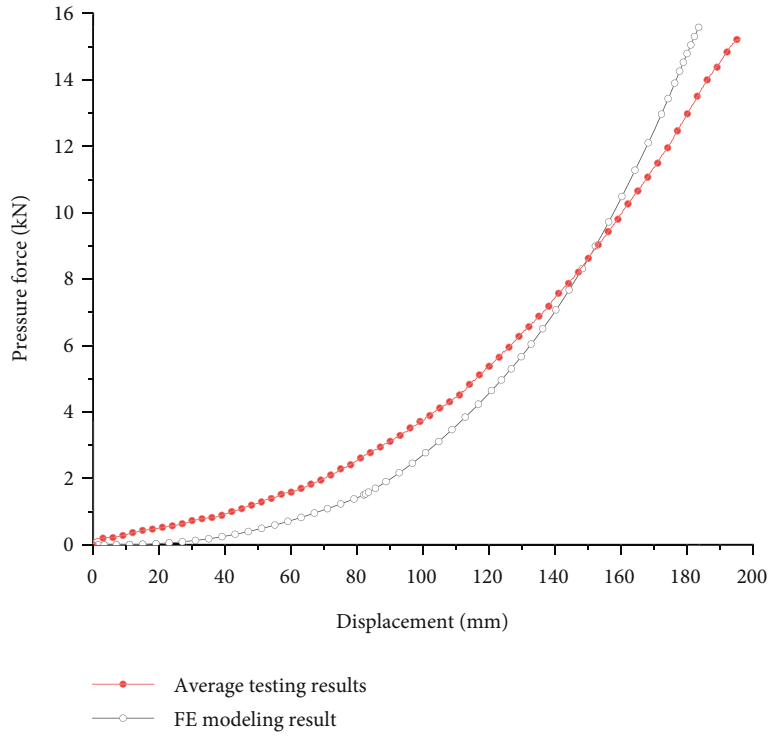

Figure 16: Pressure force vs. displacement curves obtained by the FE modeling simulation and experiments.

Table 2: The maximum displacements and peak pressure forces.

Item	Average testing results	Numerical result	Error (%)
Maximum displacement	196.28 mm	183.54 mm	6.5
Peak force	15.26 kN	15.58 kN	2.1

is the ultimate tensile stress, and σ_{lim} is equal to 1984.66 MPa; and λ is the bending moment influence coefficient considering the eccentricity geometry and the stress coefficient of the cross-section, and λ is equal to 0.20.

4.3. FE Modeling Results and Validation. The FE modeling results are compared with the experimental data to assess the reliability and accuracy of the model in predicting the behavior of the wire nets under pressure from the warhead. In particular, the deformation and fracture behavior of the wire nets, the pressure force vs. displacement curves, and the maximum displacements and peak pressure forces obtained from the FE modeling and experimental tests are discussed.

The equivalent stress contour, the deformation, and the death element location of the wire nets are shown in Figure 14. The deformation of the wire nets obtained by the FE modeling included the overall deformation, the local deformation, and the death element located in the inner connections of the center mesh. The deformation and fracture behavior of the wire nets coincided well with the experimental results (Figures 9 and 10). Figure 15 shows the stress–displacement curves of the death element, including the axial stress, total bending stress, and combined stress. At the beginning, the center mesh was mainly deformed due to eccentric stretching by the surrounding mesh, and the bending stress increased much more rapidly than the axial stress. As the center mesh expanded due to pressure from the warhead, the circumferential extrusion force increased, the axial stress increased rapidly, and the bending stress gradually decreased. Comparing the axial stress and bending stress, the axial stress is the main factor causing fracturing of the steel wire, and the axial stress accounts for 80.0% of the combined stress.

Figure 16 displays the pressure force vs. displacement curves obtained by the FE modeling simulation and experiments. The general trend of the numerical results matched well with those of the experiments. The discrepancy can be partially attributed to the initial pretensioned conditions of the wire nets and the sliding at the inner connections. In the tests, the wire nets were pretensioned before the warhead device was applied, which would increase the stiffness of the wire nets at the beginning, resulting in the pressure force being larger than that of the numerical simulation at the same displacement from 0 to 140 mm. With the increase in the displacement from 140 to 180 mm, the pressure forces obtained by the tests were lower than those obtained by the numerical simulation due to the sliding effects at connections A and C. Table 2 shows the maximum displacement and peak pressure force obtained by the tests and numerical simulation, and the maximum displacement and the peak pressure force obtained by the numerical simulation coincide closely with the experimental data. Therefore, the developed numerical approach and FE model are reliably able to predict the behavior of wire nets under pressure from a warhead device.

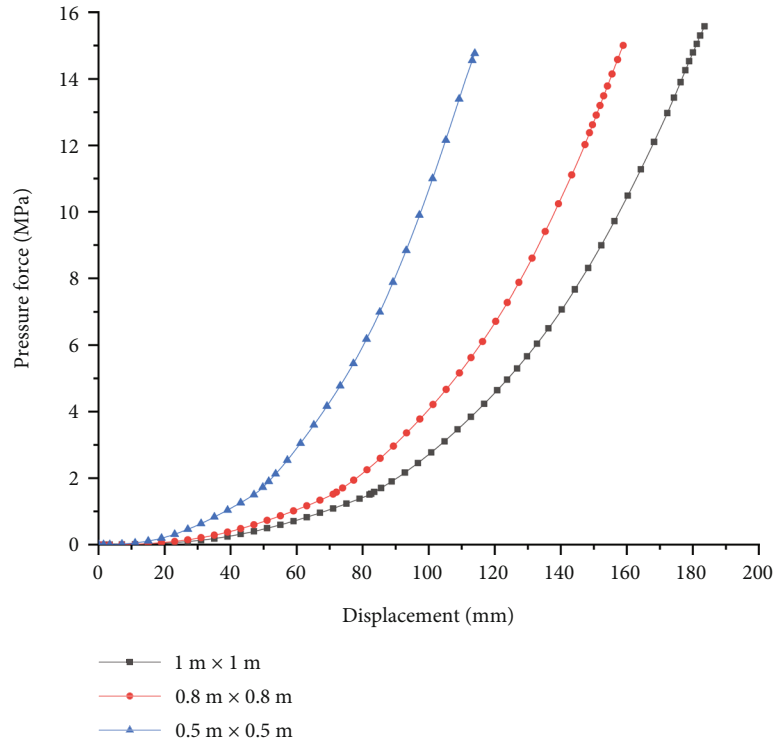

Figure 17: Pressure force vs. displacement curves of different wire net sizes.

Table 3: The changed parameters of the designed chain-link wire nets.

Item	Mesh size (mm)	Mesh angle (°)	No. of longitudinal meshes (pcs/m)	No. of transversal meshes (pcs/m)
1	$x \times y = 58.7 \times 106.1$	$\alpha = 48.9$	$n_Q = 17$	$n_L = 9$
2	$x \times y = 59.8 \times 97.5$	$\alpha = 53.9$	$n_Q = 17$	$n_L = 11$
3	$x \times y = 59.9 \times 93.0$	$\alpha = 58.9$	$n_Q = 17$	$n_L = 11$
4	$x \times y = 62.3 \times 84.5$	$\alpha = 63.9$	$n_Q = 16$	$n_L = 12$
5	$x \times y = 64.0 \times 79.5$	$\alpha = 68.9$	$n_Q = 15$	$n_L = 13$

4.4. Effects of Wire Net Size and Mesh Angle. The validated numerical approach and FE model were used to further investigate the mechanical behavior of wire nets under pressure from a warhead. The pressure force vs. displacement curves of the three wire net sizes are compared in Figure 17. The results indicate that as the wire net size decreased, the wire nets were much stiffer, which means that their force–displacement curves had steeper rising slopes, but the peak pressure force did not significantly change. Therefore, we can reduce the wire net sizes to increase the stiffness of the wire nets without considering the reduction in the peak pressure force.

The mesh angle is a key parameter when designing wire nets, and five mesh angles with the same incircle diameter of wire nets were designed. Because some of the parameters of the designed wire nets with different angles are not changed, only the changed parameters are presented in Table 3. Then, the relationships between the angle of mesh, areal density of the wire nets, and peak pressure force are analyzed by FE modeling, and the numerical simulation results are shown in Figure 18. As shown in Figure 18, the areal density and the peak pressure force increase with increasing mesh angle. To obtain a larger peak pressure force, the angle of the mesh would be close to 90°, but this would increase the areal density of the wire nets and the weaving difficulty. However, because the initial bending of the steel wire was relatively large, the initial bending stress increased, resulting in the peak pressure force rapidly decreasing when the mesh angle was less than 53.9°.

5. Conclusion and Outlook

This paper reported the mechanical behavior of chain-link wire nets under quasistatic pressure from a warhead. Quasistatic pressure tests were performed on the designed wire nets, and the deformation and fracture behavior and pressure force vs. displacement of the wire nets were investigated. Furthermore, FE modeling of the wire nets under pressure from a warhead device was developed using ANSYS 2022R1. A comparison between the numerical results and experimental data demonstrates the reliability of the numerical method and FE model in predicting the mechanical behavior of wire nets pressurized by a warhead. The effects of the wire net size and mesh angles were also investigated by using the FE model. The findings of this study can be summarized as follows:

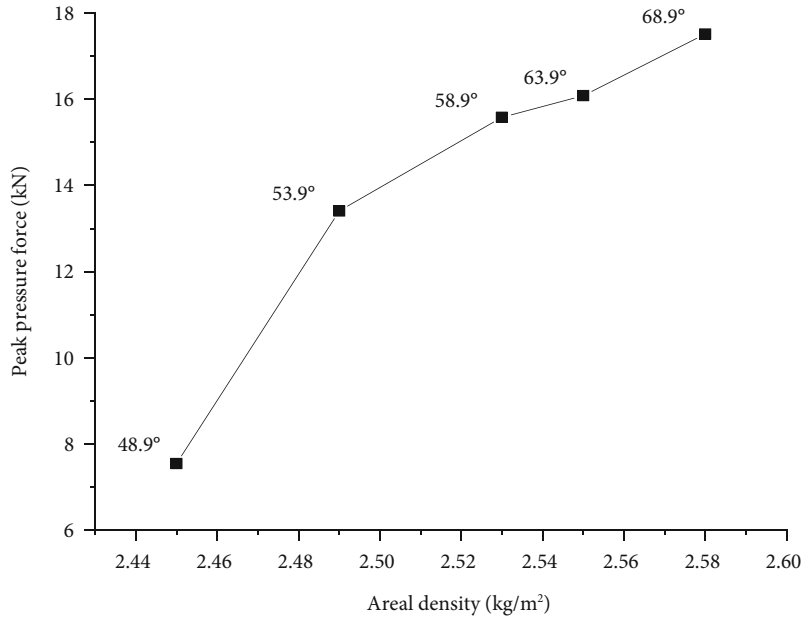

Figure 18: Areal densities of the wire nets and mesh angles vs. peak pressure force curve.

(i) The deformation of the wire nets included the overall deformation and the local deformation. The overall deformation of the wire nets fits the membrane stretching model with a funnel shape, and the local deformation referred to the expanded deformation of the center mesh impacted by the warhead device.

(ii) The fractures of the wire nets were located at the connections of the single mesh in contact with the warhead, and these phenomena were the same as those observed in the low-velocity impact tests or short-range weapon attack tests. The pressure force vs. displacement curves obtained by the tests could be identified for the initial design of the mechanical behavior of the wire nets.

(iii) The stiffness of the wire nets is related to the wire net sizes, but the peak pressure force of the wire nets under pressure from the warhead is independent of the wire net sizes. The peak pressure force is related to the mesh angle, and to obtain a larger peak pressure force, the areal density of the wire nets and the weaving difficulty would be increased. The optimal mesh angle for the incircle diameter 45 mm of the wire nets is 59.9° considering the areal density of the wire nets and the weaving difficulty.

However, the interaction between wire nets and short-range weapons is a dynamic process, and the findings presented in this paper are only the initial wire net design suggestions. The performance of high-strength steel wires and short-range weapon materials under the high strain rates, impact energy (velocity, mass), and attack angles of the weapons requires further experimental and numerical analysis.

Data Availability

The authors confirm that the data supporting the findings of this study are available within the article.

Conflicts of Interest

The authors declare that they have no conflicts of interest.

Acknowledgments

The work in this paper was supported by the Basic Reinforcement Foundation of China under Grant No. 2019-JCJQ-JJ-023 and 2020-QN-06076.

References

[1] X. H. Li, X. Zhu, R. Wang, T. Y. Li, Y. Gu, and Q. Zhang, "Experimental study on the impact resistance of hollow thin-walled aluminum alloy tubes and foam-filled aluminum tubes (6063-T5)," *International Journal of Crashworthiness*, vol. 6, pp. 1–20, 2023.

[2] X. H. Li, Y. Yin, X. Zhu et al., "Performance of hollow and aluminum foam-filled multi-cell thin-walled aluminum alloy tubes (6063-T5) under axial impact," *Structure*, vol. 47, pp. 1803–1821, 2023.

[3] D. Y. Tao, J. H. Yin, J. Q. Qin, Z. H. Zhu, and W. Q. Feng, "Large-scale physical modeling study on the interaction between rockfall and flexible barrier," *Landslides*, vol. 15, no. 12, pp. 2487–2497, 2018.

[4] J. B. Coulibaly, M. A. Chanut, S. Lambert, and F. Nicot, "Toward a generic computational approach for flexible rockfall barrier modeling," *Rock Mechanics and Rock Engineering*, vol. 52, no. 11, pp. 4475–4496, 2019.

[5] E. Blanco-Fernandez, D. Castro-Fresno, J. J. Del Coz Díaz, and J. Díaz, "Field measurements of anchored flexible systems for slope stabilisation: evidence of passive behaviour," *Engineering Geology*, vol. 153, pp. 95–104, 2013.

[6] B. Baek, E. Karampinos, and J. Hadjigeorgiou, "Understanding the impact of test configuration on welded-wire mesh

laboratory test results," *Rock Mechanics and Rock Engineering*, vol. 53, no. 11, pp. 4873–4892, 2020.

[7] C. Z. Wang, H. G. Wang, K. Shankar, E. V. Morozov, and P. J. Hazell, "On the mechanical behaviour of steel wire mesh subjected to low-velocity impact," *Thin-Walled Structures*, vol. 159, article 107281, 2021.

[8] C. Z. Wang, H. G. Wang, K. Shankar, and P. J. Hazell, "Dynamic failure behavior of steel wire mesh subjected to medium velocity impact: experiments and simulations," *International Journal of Mechanical Sciences*, vol. 216, article 106991, 2022.

[9] J. Li, C. Q. Wu, H. Hao, Y. Su, and Z. X. Li, "A study of concrete slabs with steel wire mesh reinforcement under close-in explosive loads," *International Journal of Impact Engineering*, vol. 110, pp. 242–254, 2017.

[10] J. Wu, J. G. Ning, and T. Ma, "The dynamic response and failure behavior of concrete subjected to new spiral projectile impacts," *Engineering Failure Analysis*, vol. 79, pp. 547–564, 2017.

[11] S. Balos, V. Grabulov, L. Sidjanin, and M. Pantic, "Wire fence as applique armour," *Materials and Design*, vol. 31, pp. 1293–1301, 2010.

[12] R. Marc and R. Andreas, *Firing Demonstration Vehicle Protection Systems LASSO/LEAR/EFP*, pp. 7–8, Geobrugg test report, 2013.

[13] N. Sasiharan, B. Muhunthan, T. C. Badger, S. Shu, and D. M. Carradine, "Numerical analysis of the performance of wire mesh and cable net rockfall protection systems," *Engineering Geology*, vol. 88, no. 1–2, pp. 121–132, 2006.

[14] J. J. Escallón, V. Boetticher, C. Wendeler, E. Chatzi, and P. Bartelt, "Mechanics of chain-link wire nets with loose connections," *Engineering Structures*, vol. 101, pp. 68–87, 2015.

[15] D. Castro-Fresno, J. J. del Coz Diaz, L. A. López, and P. J. García-Nieto, "Evaluation of the resistant capacity of cable nets using the finite element method and experimental validation," *Engineering Geology*, vol. 153, pp. 95–104, 2008.

[16] Y. T. Jin, Z. X. Yu, L. R. Luo, L. P. Guo, and L. J. Zhang, "A membrane equivalent method to reproduce the macroscopic mechanical responses of steel wire-ring nets under rockfall impact," *Thin-Walled Structures*, vol. 167, article 108227, 2021.

[17] J. J. del Coz-Díaz, P. J. García-Nieto, D. Castro-Fresno, and E. Blanco-Fernández, "Non-linear analysis of cable networks by FEM and experimental validation," *International Journal of Computational Mathematics*, vol. 86, no. 2, p. 313, 2009.

[18] A. Von-Boetticher and A. Volkwein, "Numerical modelling of chain-link steel wire nets with discrete elements," *Canadian Geotechnical Journal*, vol. 99, pp. 1–43, 2018.

[19] W. Zhu, W. X. Wang, W. B. Li, Q. Zhang, Y. F. Du, and Y. Yin, "Experimental and numerical study of X-type energy dissipation device under impact loads," *Journal of Constructional Steel Research*, vol. 204, no. 1–17, p. 107876, 2023.

[20] T. Yu, *Research on the Active Intercepting and Detonating Mechanism of TECCO Nets for Projectile Body*, pp. 65–68, Army Logistics Academy, Chongqing, 2019.

[21] K. J. Kang, "Wire-woven cellular metals: the present and future," *Progress in Materials Science*, vol. 69, pp. 213–307, 2015.